Available online at www.sciencedirect.com
SCIENCE DIRECT®
Journal of Catalysis 224 (2004) 417–428
JOURNAL OF CATALYSIS
www.elsevier.com/locate/jcat

Vanadium oxide supported on mesoporous SBA-15 as highly selective catalysts in the oxidative dehydrogenation of propane

Yong-Mei Liu, Yong Cao,* Nan Yi, Wei-Liang Feng, Wei-Lin Dai, Shi-Run Yan, He-Yong He, and Kang-Nian Fan *

Department of Chemistry, Shanghai Key Laboratory of Molecular Catalysis and Innovative Materials, Fudan University, Shanghai 200433, People's Republic of China

Received 17 December 2003; revised 27 February 2004; accepted 8 March 2004

Available online 17 April 2004

Abstract

The combination of different techniques (DR UV–vis, ^{51}V NMR, UV-Raman, FTIR, and H_2-TPR) in the characterization of vanadia supported on mesoporous SBA-15 catalysts shows that the dispersity and the nature of the vanadium species depend strongly on the V loading. In dehydrated catalysts with V contents lower than 2.8 wt%, vanadium is mainly in a tetrahedral environment. Higher V contents in the catalyst lead to the formation of polymeric V_2O_5-like species. Textural, SEM/TEM, and XRD results indicate that the ordered hexagonal mesoporous structure with large pore diameters of the support is retained upon the vanadium incorporation, and therefore high surface areas were obtained on the final catalysts. Vanadium species anchored to the surface show structural properties similar to those on mesoporous V-MCM and conventional V–SiO_2 catalysts, but a higher surface concentration of isolated or low polymeric VO_x species could be achieved on the V-SBA samples. The number and nature of the acid sites also change with the vanadium loading. The superior performance of the present mesoporous SBA-15 catalysts in the oxidative dehydrogenation of propane has been attributed to a higher dispersion of V species achieved on the SBA-15 support with large pore diameters as well as the low surface acidity of the catalyst.

Keywords: Supported vanadium oxide catalyst; Siliceous mesoporous SBA-15; SEM/TEM; TPR; UV–vis; ^{51}V NMR; UV-Raman; FTIR spectroscopy; Oxidative dehydrogenation of propane; Propylene

1. Introduction

Catalysts based on supported vanadium oxides have been reported to be active and selective for the oxidative dehydrogenation (ODH) of alkanes to their corresponding alkenes, but unselective combustion pathways limit alkene selectivities, particularly at high conversions [1–6]. Especially in the field of the oxidative dehydrogenation of propane to propylene, it has been well established that the limited propylene selectivity at higher propane conversions is linked with propylene adsorption on acid sites and their subsequent combustion to carbon oxides [2,7]. Thus, new efficient catalyst systems that can allow the effective production of propylene with high selectivity at higher propane conversions are highly desirable.

It is known that the catalytic behavior of supported vanadium oxide catalysts in the selective oxidation of propane depends strongly on the content of vanadium loaded on the metal oxide supports [8–10]. Isolated tetrahedral vanadium oxide species containing terminal V=O groups has been suggested as the active sites for the selective formation of propylene [2]. Actually, a clear relationship between the dispersion of vanadium oxide on the silica surface and the selectivity to propylene has been observed [10]. Both vanadium species dispersion and propylene selectivity drastically decreased for vanadia loading above 5 wt% in V_2O_5/SiO_2 catalysts [10]. Such behavior has been interpreted with a change in the molecular structure of the supported VO_x species with increasing vanadium loading. The selective isolated vanadium sites were predominantly formed at low vanadia content (below 1–5 wt%), while at higher loading polymeric species and even crystalline V_2O_5 species containing V–O–V entities, responsible for the over oxidation of propylene into carbon oxides, also developed on the silica

* Corresponding authors. Fax: (+86-21) 65642978.
E-mail addresses: yongcao@fudan.edu.cn (Y. Cao), knfan@fudan.edu.cn (K.-N. Fan).

0021-9517/$ – see front matter
doi:10.1016/j.jcat.2004.03.010

surface. The presence of polymerized vanadium species on the surface of silica not only has a detrimental influence on the propylene selectivity but also may exert a negative effect on catalyst activity, due to the presence of vanadium atoms nonaccessible to the propane reactant molecules.

From the above discussion, it is clear that in order to obtain more active and selective vanadium-based catalysts for ODH of propane one should achieve a high dispersion of the vanadium oxide species at vanadium loadings as high as possible. Therefore, great efforts have been dedicated toward the potential applications of high surface area materials as the supports for dispersing the vanadium atoms [11,12]. Recently, the new discovery of the family of siliceous mesostructured materials M41S has attracted much attention as catalyst supports since they possess high surface areas ($> 800\ m^2\ g^{-1}$) as well as well-ordered hexagonal channels with controllable uniform pore sizes of 2–8 nm [13,14]. Regarding the various synthetic methods proposed for the synthesis of active and selective vanadium-containing MCM materials without collapse of the mesoporous structure [15–20], the conventional impregnation method has appeared to be more practical and attractive to obtain the highly active and selective VO_x/MCM-41catalysts with increased amounts of vanadium species [20]. Solsona and coworkers have demonstrated that a higher concentration of isolated tetrahedral vanadium species was achieved with the MCM-41 support as compared with amorphous silica, resulting in a greater density of surface-active sites [20]. As a consequence, VO_x/MCM catalysts displayed high productivities, keeping high selectivities to propylene during the oxidative dehydrogenation of propane. Unfortunately, to the best of our knowledge, the yield of olefins from propane did not achieve above 30% over all catalyst systems reported up to now [15–20].

Very recently, SBA-15, another new type of ordered mesoporous material achieved by using a triblock copolymer as structure-directing agent under strongly acidic conditions, has also attracted great attention in the field of catalysis [21–26]. SBA-15 material possesses a high surface area ($600–1000\ m^2\ g^{-1}$) and is formed by a hexagonal array of uniform tubular channels with tunable pore diameters in the range of 5–30 nm which are significantly larger than those of MCM-41 [13]. Especially given its thicker walls (31–64 Å), SBA-15 provides a thermal stability and hydrothermal stability that exceed those for the thinner walled MCM-41 materials [27]. In a preliminary communication, we have reported that the use of mesoporous SBA-15 silica as a support can allow the generation of a highly efficient VO_x-SBA-15 catalyst (see Scheme 1, Ref. [28]) exhibiting high selectivities (80%) to olefins at high propane conversions (42%) in the oxidative dehydrogenation of propane [28]. The introduction of vanadium species onto the inner walls of SBA-15 can provide new vanadium-containing catalysts with a large concentration of accessible, isolated, and structurally well-defined active sites for the ODH of propane [29]. The superior performance of the mesoporous VO_x-SBA-15 catalyst is related to the particular large pore diameter as well as a low surface acidity achieved in the SBA-15 catalysts [28,29]. However, a fundamental understanding of the nature and redox properties of the vanadium species anchored on the surface of the SBA-15 support, especially the role of the pore diameter of the catalyst during the selective oxidation of propane, remained to be established.

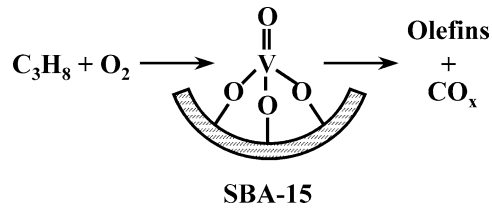

Scheme 1.

To gain a further insight into the dispersity and the nature of V species formed on SBA-15-supported vanadia catalysts (VO_x-SBA-15), a detailed characterization of the vanadium incorporated SBA-15 catalysts by SEM/TEM, DR UV–vis, ^{51}V NMR, H_2-TPR, UV-Raman, and FTIR spectroscopy as well as their catalytic performance in the oxidative dehydrogenation of propane has been presented in this paper. The nature and redox properties of the VO_x species anchored on the mesoporous SBA-15 carrier are also compared with those on MCM-41 and conventional SiO_2 support.

2. Experimental

2.1. Catalyst preparation

A purely siliceous SBA-15 sample was prepared according to a literature procedure using Pluronic P123 triblock polymer ($EO_{20}PO_{70}EO_{20}$, $M_{av} = 5800$, from Aldrich) as template under acidic conditions [21]. Briefly, a solution of $EO_{20}PO_{70}EO_{20}$:2 M HCl:TEOS:H_2O = 2:60:4.25:15 (mass ratio) was prepared, stirred for several hours at 40 °C, and then hydrothermally treated at 95 °C for 3 days. The solid products were recovered by filtering off. Then, the SBA-15 was dried overnight at 100 °C. The occluded surfactant was removed by calcination at 600 °C for 5 h in air, yielding the final mesoporous SBA-15 material.

SBA-supported vanadia catalysts were prepared by following an alcoholic impregnation method [29]. A methanol solution of NH_4VO_3 to achieve a final V content of 1.0 to 9.0 wt% of V atoms was contacted with the SBA-15 carrier at 60 °C and the methanol was rotaevaporated until complete dryness. Then, the catalysts were dried overnight in air at 120 °C, followed by calcination at 600 °C for 4 h in air. The impregnated samples named by a number (denotes the V content in the calcined catalysts) followed by SBA are summarized in Table 1. Thus, sample named 2.8V-SBA is a SBA-15-supported catalyst with 2.8 wt% of V atoms. For comparison, vanadia catalysts supported on MCM-41 and amorphous silica (from Shanghai Super Chemical Material

Table 1
Characteristics of the supported vanadia catalysts

Sample	S_{BET} ($m^2\,g^{-1}$)	V_p ($cm^3\,g^{-1}$)	D_{BJH}[a] (nm)	V density (VO_x per nm^2)	H_2-TPR results[b]		
					T_M (°C)	H_2 uptake	AOS
SBA-15	695	1.22	7.6	–	–	–	–
1.0V-SBA	592	1.09	7.1	0.21	496	160	4.63
1.8V-SBA	559	0.99	7.0	0.39	496	255	4.44
2.8V-SBA	478	0.88	6.4	0.69	504	352	4.28
4.5V-SBA	458	0.73	6.0	1.16	526	440	4.00
9.0V-SBA	448	0.75	5.2	2.40	554	1413	3.16
2.8V-MCM	985	0.56	2.7	0.34	503	316	4.15
2.8V–SiO_2	222	0.25	9.1	1.49	514	275	4.00

[a] The pore-size distribution (PSD) determined based on the BJH method.
[b] Temperature of the maximum hydrogen consumption (T_M), H_2 consumption in μmol H_2/g of catalyst, and the average oxidation state (AOS) based on H_2 consumption.

Co. Ltd., A type, 260 $m^2\,g^{-1}$) have also been prepared following the same procedure.

2.2. Catalyst characterization

Nitrogen adsorption/desorption at 77 K were measured using a Micromeritics TriStar 3000 equipment after the samples were degassed (1.33×10^{-2} Pa) at 300 °C overnight. The specific surface area was calculated following the method of Brunauer, Emmet, and Teller (BET). The method of Barret, Joyner, and Halenda (BJH) was used to determine the pore-size distribution (PSD).

X-ray diffraction patterns (XRD) were collected using a Germany Bruker D8Advance X-ray diffractometer equipped with a graphite monochromator, operating at 40 kV and 40 mA and employing nickel-filtered Cu-Kα radiation ($\lambda = 1.5418$ Å).

Scanning electron microscopy (SEM) was recorded digitally on a Philips XL 30 microscope operating at 30 kV. Before being transferred into the SEM chamber, the samples dispersed with ethanol were deposited on the sample holder and then quickly moved into the vacuum evaporator (LDM-150D) in which a thin gold film was deposited after drying in vacuo.

Transmission electron microscopy (TEM) was recorded digitally with a Gatan slow-scan charge-coupled device (CCD) camera on a JEOL 2011 electron microscope operating at 200 kV. The samples were prepared by dispersing the powder products as a slurry in acetone, which was then deposited and dried on a holey carbon film on a Cu grid.

Diffuse reflectance UV–vis spectra were collected on a Varian Cary 5 spectrophotometer equipped with a Praying Mantis attachment from Harrick. The sample cell was equipped with a heater unit, a thermocouple, and a gas flow system for in situ measurements. The samples were dehydrated in situ in dry air at 400 °C for 30 min. The spectra were recorded upon cooling down to room temperature, with dry air flowing through the sample to avoid the rehydration processes. The absorption edge energies for dehydrated spectra were determined by finding the intercept of the straight line in the low-energy rise of a plot of $[F(R_\infty)h\nu]^{1/2}$ against $h\nu$ [8,9], where $F(R_\infty)$ is a Kubelka–Munk function [30], $h\nu$ is the energy of the incident photon.

Prior to recording of the ^{51}V nuclear magnetic resonance (NMR) spectra, the samples were treated under dynamic vacuum at 100 °C overnight and then transferred and sealed into the rotor in a glove box under an atmosphere of nitrogen. Solid-state ^{51}V NMR spectra were recorded at 7.05 T at ambient temperature on a Bruker AVAVCE DSX 300 spectrometer at 78.9 MHz, using a high-speed MAS Doty supersonic probe (zirconia rotors with 5 mm in diameter). Short excitation pulses of 1 μs duration and recycle delays of 1 s were applied. The chemical shifts are given in ppm related to $VOCl_3$.

In situ laser Raman spectra were obtained using a confocal microprobe Jobin Yvon Lab Ram Infinity Raman system equipped with both UV and visible excitation lines. The UV-Raman measurements were carried out using the UV line at 325 nm from a Kimmon IK3201R-F He–Cd laser as the exciting source, where a laser output of 30 mW was used and the maximum incident power at the sample was approximately 6 mW. The sample was loaded in an in situ cell and was treated in dry airflow at 500 °C for 1 h for dehydration. All spectra were recorded at 200 °C in N_2 gas flow with a resolution of 4 cm^{-1}.

Temperature-programmed reduction (TPR) spectra were obtained on a homemade apparatus loaded with 100 mg of catalyst [31]. The samples were pretreated in flowing air at 600 °C for 2 h in order to ensure complete oxidation. Then the samples were cooled to room temperature in argon. The samples were subsequently contacted with an H_2/Ar mixture (H_2/Ar molar ratio of 5/95 and a total flow of 40 ml min^{-1}) and heated, at a rate of 10 °C min^{-1}, to a final temperature of 800 °C. The H_2 consumption was monitored using a TCD detector.

In order to characterize the acidity of the catalysts, spectra in the OH vibration region as well as spectra of chemisorbed pyridine were monitored on a Bruker Vector 22 spectrometer using self-supporting wafers in a heatable IR gas cell [32]. The samples were pretreated at 450 °C for 1 h under vacuum prior to pyridine adsorption. Pyridine was adsorbed at room temperature from an argon flow containing 2 vol% pyri-

dine. Then, the samples were heated to 100 °C and evacuated to remove physisorbed and weakly chemisorbed pyridine. Temperature-programmed desorption of the adsorbed pyridine starting at 100 °C was studied by stepwise heating of the sample under vacuum to characterize the strength of the acid sites. Difference spectra were obtained by subtracting the background (base spectrum) of the unloaded sample.

2.3. Catalytic tests

The catalytic experiments were carried out in a fixed-bed quartz tubular flow reactor (i.d. 6 mm, length 400 mm) at atmospheric pressure [29,31]. The reactor was equipped with a coaxial thermocouple for catalytic bed temperature monitoring. Catalyst samples (60–80 mesh) were introduced into the reactor and diluted with 300 mg quartz powder (40–60 mesh) to keep a constant volume in the catalyst bed. The flow rate and the amount of the catalyst were varied to achieve different propane conversion levels. The feed consisted of a mixture of propane/oxygen/nitrogen with a molar ratio of 1/1/4. Experiments were carried out at 600 °C to achieve the higher selectivity to partial oxidation products. The feed and the reaction products were analyzed on-line by online gas chromatograph (Type GC-122, Shanghai). Permanent gases (N_2, O_2, CO, CO_2) were separated using a TDX-01 column connected to a TCD detector and other reaction products were analyzed employing a Porapak Q column connected to a FID detector. Blank runs show that under the experimental conditions used in this work the homogeneous reaction could be neglected.

3. Results

3.1. Catalysts characterization

SBA-15-supported vanadia samples (V loadings from 1.0 to 9.0 wt%) present well-defined XRD patterns corresponding to SBA-15 structures (Fig. 1), implying that all catalysts prepared by alcoholic impregnation have ordered hexagonal mesostructures. However, a shift of the diffraction peaks to higher 2θ values is identified for the V-SBA samples, possibly due to a contraction of their frameworks with increasing vanadium loading during the calcination procedure [29]. Moreover, it is seen that the intensity of the d_{100} peak is gradually attenuated (inset to Fig. 1) with increasing V loading in the XRD patterns of the samples. The reduction of the reflections may be caused by a degradation of the hexagonal arrangement of SBA-15 pores [12,20]. The hexagonal arrangement of the SBA-15 frameworks was retained after vanadia incorporation, as could be seen from TEM and N_2-adsorption data presented as follows. Thus, the progressive reduction of the d_{100} reflections in the present case is more likely due to a dilution of silica with continuous incorporation of vanadia as a consequence of higher absorption factor for X-rays than silicon [26]. The absorption of X-rays

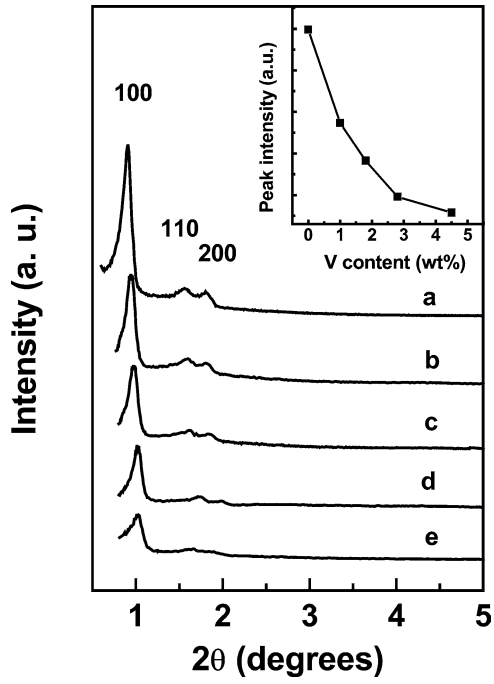

Fig. 1. Low-angle X-ray diffraction patterns of calcined SBA-15-supported vanadia catalysts: (a) SBA-15; (b) 1.0V-SBA; (c) 2.8V-SBA; (d) 4.5V-SBA; (e) 9.0V-SBA.

by vanadia was indeed very significant, as inferred from strong reduction of the main beam intensity.

SEM image (Fig. 2a) reveals that the as-synthesized parent SBA-15 sample consists of well-defined wheat-like macro-structures aggregated with rope-like domains with relatively uniform sizes of 1 μm [21]. After vanadium incorporation, a significant degradation in macroscopic structure occurred; however, the rope-like domains with average sizes of 1 μm were still largely maintained (Figs. 2c anf 2e). TEM images (Figs. 2b, 2d, and 2f) of all SBA-15 samples (including different V loadings) show well-ordered hexagonal arrays of mesopores (1D channels) and unambiguously confirm that the hexagonal pore structure of the SBA-15 was robust enough to survive the vanadium incorporation process and so offers a good matrix to support highly dispersed vanadium species.

The maintenance of ordered hexagonal arrangement of the SBA-15 frameworks upon vanadium introduction is further supported by the N_2-adsorption data. Although the incorporation of vanadia into SBA-15 led to a continuous decrease of the specific surface area and the cumulative pore volume (Table 1), high surface areas (S_{BET}) and pore volumes as well as very narrow pore-size distributions are observed in SBA-15-supported materials with V loading up to 9 wt%. A similar decrease of the S_{BET} and pore volume has already been reported by Berndt et al. for mesoporous V-containing MCM materials [33]. Thus, it can be concluded that well-organized mesoporous SBA-15 catalysts with a high surface area could be obtained at all V loadings in the present study.

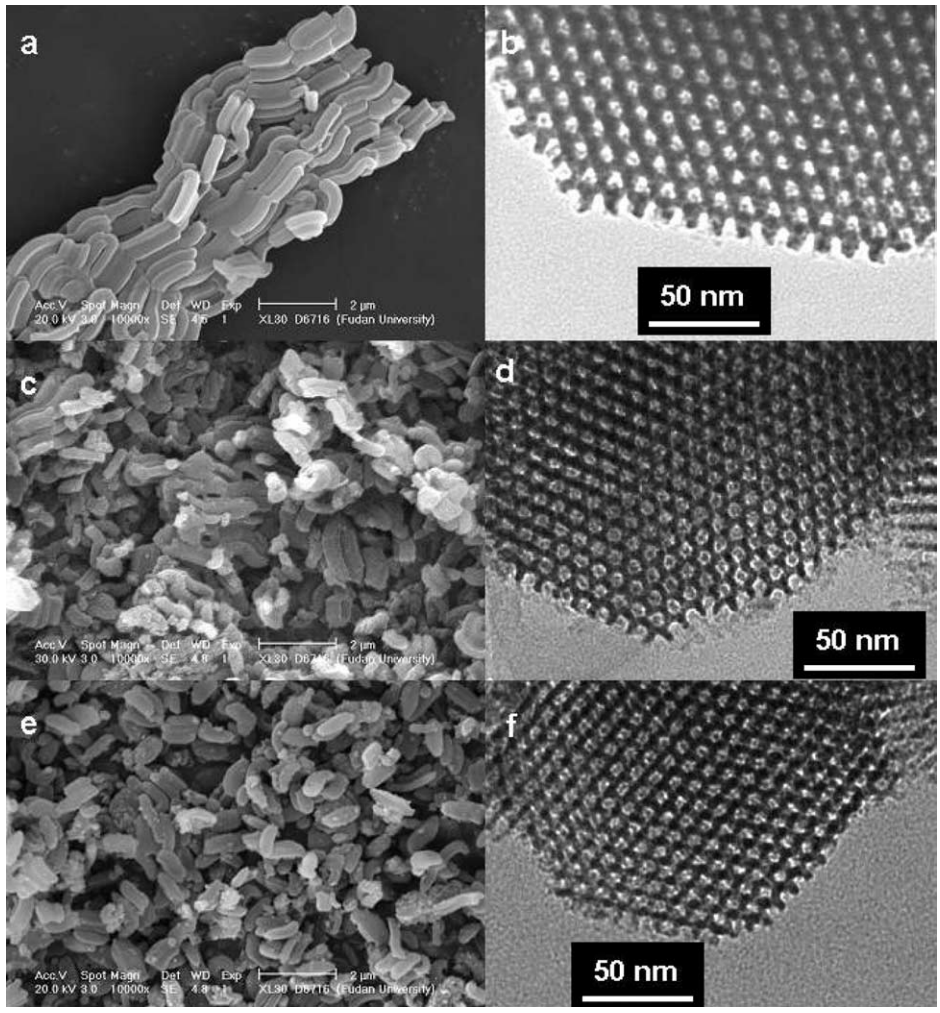

Fig. 2. SEM (a, c, e) and TEM (b, d, f) images of various V-containing SBA-15 samples: (a, b) parent SBA-15; (c, d) 2.8V-SBA; (e, f) 9.0V-SBA.

Considering that the nature of the vanadium supported on siliceous materials is highly moisture sensitive [34–36], to identify the exact vanadium environment, diffuse reflectance spectra in the UV–vis region of SBA-15-supported samples were recorded in the dehydrated state. Fig. 3 shows the diffuse reflectance UV–vis spectra of calcined VO_x/SBA samples after dehydration under dry air at 450 °C (Fig. 3A) and after rehydration at room temperature (Fig. 3B), the absorption edge energies for dehydrated spectra are also included. In the dehydrated samples, a decrease of the energy with increasing vanadium content is identified, reflecting an increase in the size and dimensionality of VO_x domains as vanadium surface density increases [8,9]. The presence of a very broad band centered at ca. 300 nm is also observed. A deconvolution of this band reveals two main absorption features at 250 and 320 nm corresponding to isolated V sites in tetrahedral coordination and polymeric V–O–V species, respectively [20,33,35–38]. As the vanadium content increases, one can observe an increase of the intensity of the band at 320 nm with respect to the absorption appearing at 250 nm, resulting in a progressive shift of the overlapping band toward a higher wavelength. In addition, a new feature at 450 nm appears for the samples with 4.5 wt% V loading, pointing to the presence of "bulk-like" V_2O_5 crystallites due to a further polymerization of the V species [20, 35–38]. The presence of these three bands has also been reported in vanadia catalysts supported on MCM-41 or silica [20,35–38]. Thus, the present observation of the increase of the relative intensities of the absorptions at 320 and 450 nm with increasing vanadium content can be attributed to the presence of vanadium species with a larger polymerization degree at high V loadings.

^{51}V NMR has been shown to be a powerful technique in the characterization of the local coordination environment of V^{5+} cations in the supported vanadium oxide catalysts. Comparisons of the NMR spectra of the catalysts with model compounds can a provide an opportunity to extract additional information about the symmetry environment of vanadium sites in the vanadium-containing SBA-15 catalysts [39,40]. Fig. 4 shows the ^{51}V wide-line NMR spectra of calcined 2.8V-SBA and 4.5V-SBA catalysts dehydrated and after hydration by exposing them to ambient air for 2 days. The NMR spectra of the dehydrated catalysts 2.8V-SBA (Fig 4a) and 4.5V-SBA (Fig. 4c) consist of a resonance at ca.

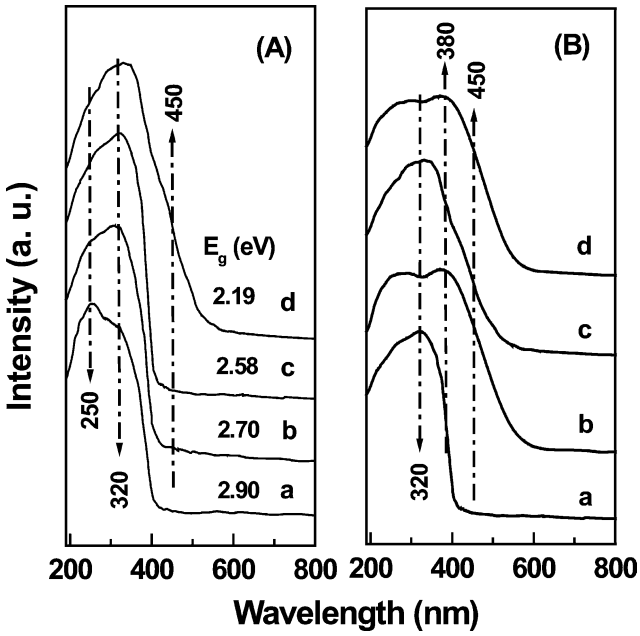

Fig. 3. Diffuse reflectance UV–vis spectra of (A) calcined SBA-15-supported vanadia catalysts after dehydration at 450 °C in air for 2 h: (a) 1.0V-SBA; (b) 1.8V-SBA; (c) 2.8V-SBA; (d) 4.5V-SBA. (B) calcined catalysts prior to and after hydration: (a) 2.8V-SBA-dehydrated; (b) 2.8V-SBA-hydrated; (c) 4.5V-SBA-dehydrated; (d) 4.5V-SBA-hydrated.

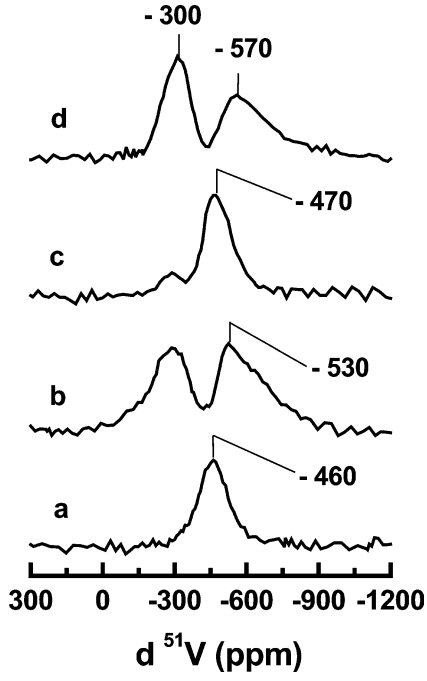

Fig. 4. ^{51}V wide-line NMR spectra of dehydrated (a, c) and hydrated (b, d) 2.8V-SBA (a, b) and 4.5V-SBA (c, d) catalysts.

−460 and −470 ppm, respectively, which can be attributed to distorted isolated tetrahedral V^{5+} of type $(SiO)_3$–V–O, in agreement with previous studies on VO_x/SiO_2 [40,41] and V-containing mesoporous MCM materials [20,33,35]. However, on consideration of the UV–vis results, the contribution of low polymeric V^{5+} sites to the NMR signals of the dehydrated 2.8V-SBA (Fig. 4a) and 4.5V-SBA (Fig. 4c) cannot be excluded. A weak signal at −300 ppm appears in the spectrum of the dehydrated sample 4.5V-SBA (Fig. 4c), which is generally assigned to the V^{5+} in a distorted octahedral or pseudo-octahedral symmetry as in V_2O_5 [20,39]. The existence of octahedral V^{5+} after dehydration could be due to the formation of a "bulk-like" surface oxide phase at higher vanadium content.

After hydration, two main signals, at −300 ppm and another one at ca. −530 and −570 ppm for 2.8V-SBA (Fig. 4b) and 4.5V-SBA (Fig. 4d), respectively, are registered in the NMR spectra. In agreement with previous publications the wide-line spectrum can be interpreted as the contribution of two different signals [39,42,43]. The low-field peak in the spectra indicates the presence of vanadium in octahedral coordination; however, due to distortion of the spectrum we cannot establish the symmetry of this octahedral site [44]. The appearance of this signal after hydration suggests that a part of the tetrahedral vanadium coordinates to two (or one) extra water molecules to produce octahedral (or pseudo-octahedral) coordination. This species is proposed to be of the $(SiO)_3$–V=O$(H_2O)_2$ type for isolated V^{5+} species [20]. This suggestion is further supported by comparing the UV–vis spectra of the dehydrated 2.8V-SBA and 4.5V-SBA catalysts with those obtained in their rehydrated state, where it can be seen that upon hydration a new band at 380 nm appears which can be unambiguously assigned to pseudo-octahedrically coordinated V^{5+} species as a consequence of the interaction of tetrahedral sites with two molecules of water [20]. Interestingly, the presence of the absorption at 320 nm in the UV–vis spectra of the hydrated samples suggests that a portion of the V species remains in pure tetrahedral coordination. This indicates the existence of nonaccessible tetrahedral V species incorporated within the pore walls of the siliceous SBA-15 structure, in accordance with previous studies on V-containing mesoporous MCM materials [20,33]. The second signal, characterized by a maximum between −500 and −600 ppm (at ca. −530 or −570 ppm) possessing a low anisotropy of the chemical shift, dominates the wide-line spectrum. Comparison with model compounds allows us to attribute this signal to the presence of polymeric tetrahedral vanadium sites [39,40], although it appears at a different position from that in the dehydrated catalysts.

UV resonance Raman spectroscopy has recently been shown to be another powerful technique for the study of various catalytic materials, especially for the identification of the molecular structure of isolated transition metal atoms anchored on the surface of metal oxides [45–49]. The resonance Raman effect may provide opportunity to selectively enhance the intensity of the Raman signal by several orders of magnitude when the excitation laser line is close to the electronic transition absorption of the samples [46]. Fig. 5 shows the UV-Raman spectra excited by a 325-nm line of the V-containing samples, which are significantly different from the visible Raman spectra as previously reported [29]. The measurements were performed at 200 °C in N_2 gas flow

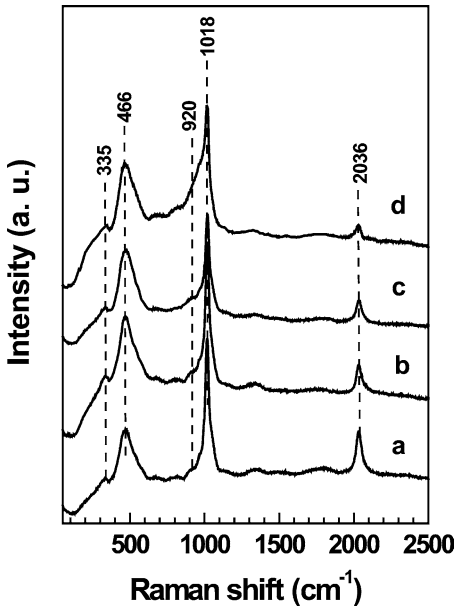

Fig. 5. In situ UV-Raman spectra of SBA-15-supported vanadia catalysts: (a) 1.0V-SBA; (b) 2.8V-SBA; (c) 2.8V-MCM; (d) 2.8V–SiO_2.

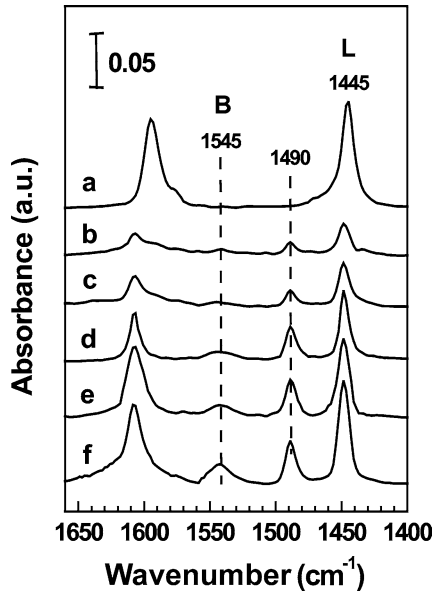

Fig. 6. FTIR sectra of pyridine adsorbed on the samples: (a) SBA-15; (b) 1.0V-SBA; (c) 1.8V-SBA; (d) 2.8V-SBA; (e) 2.8V-MCM; (f) 2.8V–SiO_2.

to keep the sample dehydrated since it was clarified that the hydration of the V-containing samples would greatly affect the Raman spectra. As shown in Fig. 5, the Raman bands at 336, 466, 920, 1018, and 2036 cm^{-1} are observed for the V-SBA samples with V content of 1.0 and 2.8 wt%. The band at 460 cm^{-1} is associated with the vibration of the siloxane rings of siliceous SBA-15 [49]. The 335 and 920 cm^{-1} bands are assigned to the bending mode of the V–O–V bond and symmetric OVO stretching of the polymeric vanadia species, respectively [47,50]. The 1018 cm^{-1} band is attributed to the symmetric stretching mode of the V=O bond of the isolated tetrahedral VO_4 species anchored on SBA-15. The bands at 1018 and 2036 cm^{-1} are, respectively, the fundamental and double-frequency bands of the tetrahedral V=O bonds because the frequencies of the latter are approximately double at 1018 cm^{-1} [48]. To the best of our knowledge, the 2036 cm^{-1} band was never detected in visible Raman spectra for supported vanadia because there is no resonance effect in the visible region.

The absence of a typical band at ca. 990 cm^{-1} of V_2O_5 in Fig. 5a and 5b implies that no crystalline V_2O_5 is formed in V-SBA samples with V content lower than 2.8 wt%. This suggests that the vanadium species in V-SBA samples are isolated or, at least, highly dispersed on the surface [29]. In comparison, an additional shoulder band at ca. 990 cm^{-1} was observed in Fig. 5c for the 2.8V–SiO_2 and 2.8V-MCM samples, suggesting the existence of crystalline V_2O_5 in these two samples. On the other hand, a decrease in the relative intensity for the V=O overtone stretching with respect to the fundamental frequency band of the V=O band has been observed for the V-SBA sample with increasing V content. As the Raman band intensity of an absorbing sample is known to be a balance between the extent of resonance enhancement and the number of supported metal oxide species excited by the laser, if the extent of resonance enhancement was insufficient to overcome the effect of the reduced number of the scatters, a decrease in Raman band intensity would occur for the samples that are transparent or weakly absorbing in the visible and strongly absorbing in the ultraviolet [47]. Thus, the present observation of the decrease in the relative intensity for the V=O overtone stretching with increasing vanadium content over V-SBA samples is possibly due to a negative effect of enhanced absorption in the ultraviolet region by the 2.8V-SBA sample as a consequence of fewer scatters sampled by the laser beam [47]. It is worth noting that a variation of the relative intensity for the V=O overtone stretching with respect to the fundamental band has also been identified for the vanadium (2.8 wt%) catalysts supported on siliceous SBA-15, MCM-41, and amorphous SiO_2, further confirming the different polymerization degree of dispersed vanadia species achievable over the different siliceous materials.

Pyridine adsorption was followed by infrared spectroscopy to identify the number and nature of acid sites in SBA-15-supported catalysts. Fig. 6 shows the FTIR spectra of the catalysts after pyridine adsorption and subsequent evacuation at 150 °C. In the spectrum of the parent SBA-15 a band at 1445 cm^{-1} appears and is assigned to pyridine coordinatively bound to defect sites of a distorted silica network as weak acidic Lewis sites [51], or to hydrogen-bonded pyridine [52]. The spectrum of the two catalysts with vanadium content lower than 2.8 wt% additionally show a weak band at 1545 cm^{-1} which can be attributed to pyridine cations formed on acidic V–OH groups (Brønsted sites) [33]. The presence of a single V–O–Si bridge and two V–OH groups for vanadium oxide species anchored to the wall of

the MCM-41 has been previously discussed by Grubert et al., who studied the reduction mechanism of VO_x species on MCM-41 [53]. Additional bands at 1490 and around 1600 cm^{-1}, associated with the presence of pyridine, are also observed in all the catalysts. However, their assignment to a specific type of acid sites is not clear [33]. Moreover, it is found that the Lewis acid sites due to parent SBA-15 decrease substantially upon the initial anchoring of vanadium onto the support surface. Nevertheless, it is seen that the number of acid sites increases with increasing vanadia content for the vanadium-containing catalysts, suggesting the formation of new type of Lewis acid sites on the V-SBA-15 samples. Thus, for the SBA-15-supported vanadia catalysts studied here, the number of both Lewis acid sites and Brønsted acid sites increases with vanadium loading. According to this and based on previous results, it can be concluded that both the Lewis acid sites and the Brønsted acid sites evidenced over the V-SBA catalysts are related to vanadium oxide incorporation.

Meanwhile, a close comparison of the spectra for the 2.8V-SBA sample with those for 2.8V-MCM and 2.8V–SiO_2 catalysts in Fig. 6 reveals that at the same V loading level the total number of both the Lewis acid sites and Brønsted acid sites is much lower on the SBA-15 catalyst than its MCM-41 or conventional SiO_2 counterparts. Moreover, the temperature-programmed pyridine desorption showed that pyridine adsorbed on V-SBA samples was completely removed at 200 °C already. In contrast, the complete removal of the pyridine adsorbed on V-containing MCM-41 and conventional SiO_2 samples could only be achieved at temperature well above 250 °C. Thus, the temperature-programmed pyridine desorption reveals a relatively moderate acid strength of the Brønsted and Lewis sites on the V-SBA catalysts.

The TPR profiles of V-SBA catalysts are comparatively shown in Fig. 7 and their main features summarized in Table 1. One sharp peak at ca. 500 °C is observed on SBA-supported samples with V loadings from 1.0 to 2.8 wt%. In the sample with high V content (4.5V-SBA) the main peak becomes broader and shifted to 526 °C with a shoulder appearing at 590 °C (Fig. 7d). By analogy with previous studies on the reducibility of VO_x/SiO_2 and V-containing mesoporous materials [5,17,33,36], the peak at low temperature is attributed to the reduction of dispersed tetrahedral vanadium species, while the peak at 590 °C to the reduction of polymeric V^{5+} species V_2O_5-like. The progressive shift of the maximum of the H_2 consumption peak to high temperature with the V loading suggests a progressive formation of less reducible high polymeric vanadium species.

Moreover, the high temperature shoulder at 590 °C is also identified in the sample 2.8V-MCM (Fig. 7e), which is more evident for the 2.8V–SiO_2 sample (Fig. 7f), suggesting the presence of V_2O_5-like polymeric vanadium species over these two samples. This observation is in sharp contrast to the reduction pattern as observed for sample 2.8V-SBA (Fig. 7c). Thus, the present H_2-TPR results further confirm

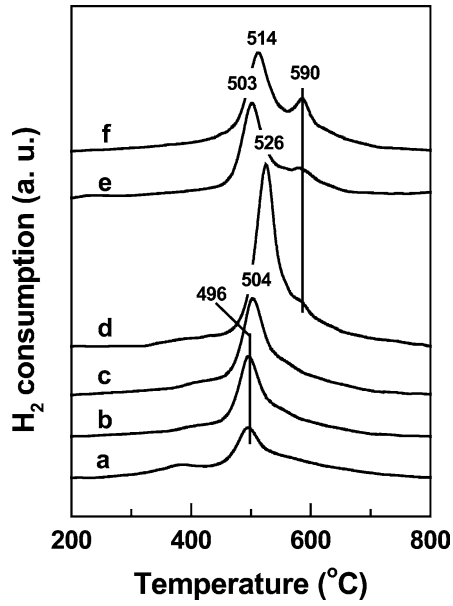

Fig. 7. H_2-TPR results of SBA-15-supported vanadium oxide catalysts: (a) 1.0V-SBA; (b) 1.8V-SBA; (c) 2.8V-SBA; (d) 4.5V-SBA; (e) 2.8V-MCM; (f) 2.8V–SiO_2.

that the formation of highly dispersed vanadium species is more favored over the surface of SBA-15. On the other hand, in consideration of a total V^{5+}-to-V^{3+} reduction for every H_2 molecule consumed, the average oxidation state (AOS) after H_2 reduction has been calculated and included in Table 1. It can be seen that the average oxidation state of vanadium in the reduced catalysts decreases as the V loading increases, and a sharp decrease of the AOS value from approximately 4 to 3 is observed for sample 9.0V-SBA. These results strongly suggest that "bulk type" V_2O_5 species could be reduced to a greater extent than isolated tetrahedral vanadium sites [33].

3.2. Catalytic tests in oxidative dehydrogenation of propane

The catalytic results obtained in the oxidative dehydrogenation of propane at 600 °C over SBA-15-supported vanadium oxide catalysts are shown in Table 2. Propylene, and carbon oxides (CO and CO_2) were the main reaction products during the ODH of propane on SBA-supported vanadia catalysts (Table 2). It is observed that propane could only be poorly converted over parent SBA-15, whereas the introduction of V remarkably enhanced propane conversion and the selectivity for partial oxidation products [28,29]. Propylene is formed with high selectivity over the SBA-15 catalysts with higher V content and the propylene yield is comparable with that obtained over V–Mg–O catalysts [6]. As shown in Table 2, the SBA-15 catalysts with low V contents would result in the formation of an appreciable amount of acrolein. Similar catalytic behavior has been observed over V catalysts supported on mesoporous silica such as MCM-41 and HMS [5,12]. It should be noted that ethylene was also

Table 2
Oxidative dehydrogenation of propane on the supported vanadia catalysts at 600 °C

Catalyst	C_3H_8 conversion (%)[a]	Selectivity (%)				C_3H_6 yield (%)	Light olefins yield (%)[b]
		C_3H_6	C_2H_4	Oxygenates [b]	CO_x[c]		
SBA-15	9.3	22.6	2.9	4.4	70.0	2.1	2.4
1.0V-SBA	34.2	46.5	9.3	6.8	30.5	15.9	19.1
1.8V-SBA	37.4	53.1	11.0	3.5	21.4	19.9	24.0
2.8V-SBA	41.7	57.0	22.8	–	9.4	23.8	33.3
4.5V-SBA	34.5	52.0	5.7	–	36.0	17.9	19.9
9.0V-SBA	33.8	48.4	4.3	–	33.8	16.3	17.8
2.8V-MCM	30.6	57.5	7.4	–	22.9	17.6	19.8
2.8V–SiO_2	25.7	54.3	4.6	1.9	28.1	13.9	15.1

[a] Reaction conditions: $W = 0.15$ g, GHSV $= 1677\ h^{-1}$.
[b] Partial oxygenated products, i.e., acrolein and trace amount of acetaldehyde.
[c] CO_x products, i.e., CO_2 and CO; light olefins, i.e., C_3H_6 and C_2H_4.

yielded in substantial amounts over V-SBA samples via oxidative cracking of propane [29]. It is remarkable that olefin selectivity up to 80% at a high propane conversion of 41.7% could be achieved over the catalyst of 2.8V-SBA.

It is also clear from Table 2 that the 2.8V-SBA catalyst exhibited much higher propane conversion and selectivity to olefins than those of mesoporous 2.8V-MCM and amorphous 2.8V–SiO_2. The high selectivity to olefins on the former could be related to their highly dispersed vanadium species on the large surface of SBA-15 with a large pore diameter as described above. In a comparison of three different silica supports, it is observed that mesoporous silica (MCM-41 and SBA-15) with high surface area are more effective, as demonstrated by the higher activities observed for these supports. Additionally, with a similar V content, SBA-15 is much superior to MCM-41 as a support.

The catalytic activity of the V-SBA catalysts is found to be strongly dependent on the reaction temperature. It is known that high reaction temperatures favor higher selectivities to olefin products when the ODH reaction is carried out on V-containing catalysts. As a result, the reaction was mainly studied at 600 °C. Fig. 8a shows the variation of propane conversion with the V loading. It can be seen that propane conversion initially increases with the incorporation of vanadium, whereas the highest activity for propane conversion is achieved on the catalyst with vanadium content of 2.8 wt%. The turnover frequencies (TOF) of the olefin product of propylene and ethylene with the V loading are also compared in Fig. 8. It can be seen that the intrinsic rates of formation for propylene decreases with the vanadium loading (Fig. 8b). In comparison, a remarkably different variation behavior (Fig. 8c) with increasing V-containing has been observed for the intrinsic rates of formation for ethylene. The TOF value for ethylene formation shows a maximum on catalysts with vanadium content of 2.8 wt%, demonstrating that the ethylene formation via the oxidative cracking of propane could be achieved much more efficiently over the 2.8V-SBA catalyst.

To further investigate the influence of the vanadium contents on the catalytic behavior of the SBA-15 catalysts, the variation of the selectivities to the main products with vanadium loading at 600 °C and a propane conversion of 40% is illustrated in Fig. 9. It is interesting to find that the selectivity to propylene and ethylene shows a maximum on catalysts with a vanadium content of 2.8 wt%, which is quite different from the results obtained over V-HMS [12] or V-MCM-41 catalysts reported by Solsona et al. [20]. However, the selectivity to carbon oxides (CO_x) changes in a different way by attaining the lowest value over the 2.8V-SBA catalyst. This unique behavior for the selectivity to the undesirable deep oxidation products (CO_x) implies that the vanadium surface density is a quite important parameter for tuning the behavior of the selective oxidation of propane over the vanadia species supported on mesoporous SBA-15.

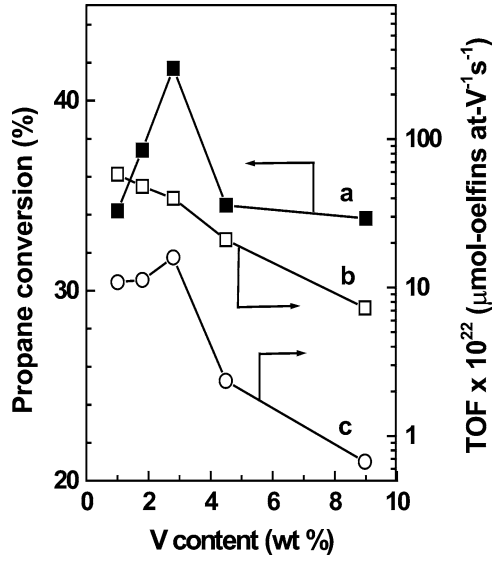

Fig. 8. Variation of the rate of propane conversion and turnover frequency (TOF) with the vanadium surface densities. Reaction temperature = 600 °C. (a) Propane conversion; (b) TOF value for propylene formation; (c) TOF value for ethylene formation.

Fig. 10 compares the variation behavior of the selectivity to propylene with the propane conversion on the vanadia dispersed on the three different siliceous supports at the same V loading level of 2.8 wt%. It is seen that the selectivity to propylene decreases with the propane conversion on all

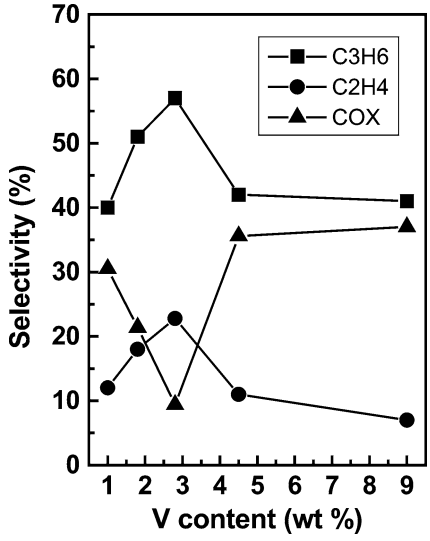

Fig. 9. Variation of the selectivity to propylene (■), ethylene (●), and CO_x (▲) with the vanadium surface densities. Reaction temperature = 600 °C; propane conversion = 40%.

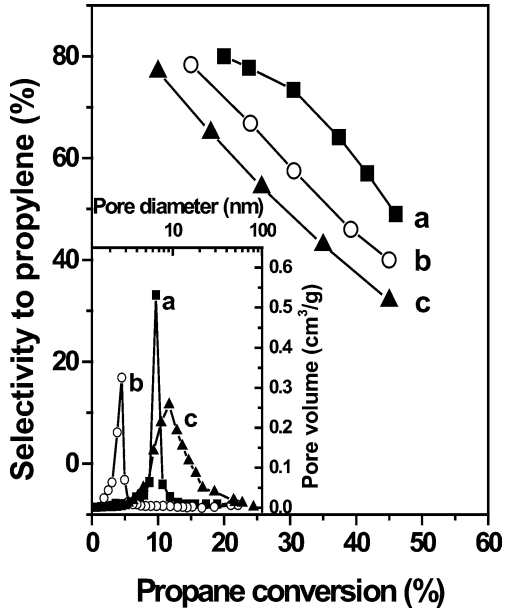

Fig. 10. Variation of the selectivity to propylene with the propane conversion obtained during the oxidation of propane at 600 °C on supported vanadia catalysts. Catalysts: (a) 2.8V-SBA; (b) 2.8V-MCM; (c) 2.8V–SiO_2. Inset shows the pore-size distribution (PSD) of the corresponding samples.

V-containing samples. By correlation with the pore-size distribution data included in the inset to Fig. 10, it could be found that the V-containing mesoporous SBA-15 is more active and selective with respect to V-MCM-41 or V–SiO_2 catalysts because its favorable large mesopore diameter limits the consecutive reaction of propylene or allylic intermediates leading to deep oxidation. In a recent adsorption equilibrium investigation of the diffusion of light hydrocarbons on silica gel, Grande and Rodrigues demonstrated that the mass transfer of propylene in the narrow-pore silica gel with average pore diameter of 4 nm was mainly controlled by Knudsen diffusion [54]. Assuming a calculation of the Knudsen diffusivity (D_k) for propylene diffusion by $D_k = 9700\, r_p (T/M)^{1/2}$, where r_p is the pore radius and M is the molecular weight of the adsorbate, the mesoporous catalyst with a larger pore diameter would have a larger D_k value for propylene diffusion, thus favorable for the discharging of the produced propylene to the outside of the pore, consequently preventing the subsequent deep oxidation.

4. Discussion

In this work a novel catalyst system VO_x-SBA-15 prepared by using well-organized hexagonal mesoporous siliceous SBA-15 as the support for the oxidative dehydrogenation of propane has been investigated in detail. Previous reported results show that the incorporation of vanadium in mesoporous MCM-41 or HMS materials allows the dispersion of a higher amount of isolated and low polymeric vanadium species on the support surface as compared to the conventional SiO_2 support, thus leading to an improved selectivity to propylene during the oxidative dehydrogenation of propane [12,33]. The present results show that the amount of dispersed vanadium ions can be further increased on SBA-15, thus yielding a more selective vanadium-based catalyst for ODH of propane.

Investigation by means of UV–vis diffuse reflectance spectroscopy has confirmed that at low V content (below 2.8 wt%), the surface of V-SBA is mainly covered by highly dispersed tetrahedral V^{5+} species and low polymeric V–O–V entities. At higher V loading, polymeric vanadium species become more abundant, and at 4.5 wt%, octahedral V^{5+} forming the oxide phase also appears. The ^{51}V NMR results of the dehydrated 2.8V-SBA and 4.5V-SBA catalysts confirm that most vanadium cations are tetrahedrally coordinated and that a V_2O_5-like phase begins to appear in the 4.5V-SBA sample. The ^{51}V MAS NMR and UV–vis spectra of the samples recorded under ambient conditions show that most vanadium species are able to coordinate additional water molecules and therefore are located in easily accessible sites. The vanadium species remaining in tetrahedral coordination in the presence of moisture has been attributed to nonaccessible V^{5+} cations buried in the framework of the pore walls. Similar UV–vis and ^{51}V MAS NMR spectra have been reported previously in V-containing MCM-41 or V-substituted MCM-41 [5,17,20, 55,56] and also on SiO_2-supported vanadia [10,57,58] or V-silicate [32,59,60]. Therefore, the nature of the vanadium species formed on siliceous or mesoporous SBA-15 supports must be similar.

The TPR results show that the reducibility of the isolated V^{5+} species anchored on the pore walls of the SBA-15 support, which are predominant at low V content, is similar to that reported for this species on MCM-41 and SiO_2 [10, 20,56–58]. Polymeric V^{5+} species and/or V_2O_5 crystallites, formed on catalysts with V loading higher than 2.8 wt%,

are more difficult to reduce. Again, the reducibility behavior of vanadium oxide supported on mesoporous SBA-15 suggests that the same type of vanadium species observed on V-MCM-41 and V–SiO_2 catalysts is formed on SBA-15 support. Such a result is consistent with the conclusion from UV–vis and ^{51}V MAS NMR measurements described above.

Compared to the visible Raman spectra as reported in our preceding paper [29], the present UV-Raman spectra of the V-SBA samples show significant differences in the 850–1050 cm^{-1} range. The intense Raman band at 1018 cm^{-1} associated with the terminal V=O stretches of isolated tetrahedral VO_4 species in the present UV-Raman spectra has a different band position as the relatively weaker band at 1036 cm^{-1} observed in visible Raman spectra for the V-SBA samples [29]. The difference in Raman shift of these two bands could be due to two type of mono-oxo vanadium species, and the species with a V=O stretch at a lower Raman shift is preferentially resonance enhanced under UV excitation [46]. A similar observation for the presence of three kinds of tetrahedral V^{5+} species has recently been reported by Dzwigaj et al. [61], where a combined DR UV–vis and photoluminescence spectroscopic investigation has been employed to distinguish the different kinds of tetrahedral vanadium species incorporated in VSiβ zeolites. On the other hand, according to the empirical relationship between V=O bond lengths and Raman stretching frequencies, a lower frequency corresponds to longer V=O bonds [48]. Therefore, the present band with a lower frequency at 1018 cm^{-1} corresponds to a longer V=O bond distance, providing evidence for the presence of isolated mono-oxo vanadate species of a tetrahedral structure with a weaker structural tension. This structure could be preferentially resonance enhanced by the 325-nm line excitation, thus leading to the appearance of well-defined overtone bands characteristic of the V=O bond at ca. 2036 cm^{-1}.

Characterization by FTIR/pyridine adsorption has confirmed the formation of V–OH groups corresponding to weak acidic Brønsted sites as well as the generation of new Lewis acid sites over the vanadium-containing V–SBA samples. This result indicates that incorporation of vanadium provokes a moderate development of acidity [5]. Moreover, the temperature-programmed pyridine desorption reveals that both the strength and the density of the acid sites on the V-SBA sample are much weaker/or lower compared with the V-MCM and V–SiO_2 samples, suggesting the weak nature of the acid sites developed on the V-loaded SBA-15 catalysts. Takehira and co-workers have proposed that the formation of deep oxidation products (CO_x) is closely related to the interaction of propylene or allylic intermediates with surface medium acid sites during the ODH of propane over MCM-41-supported vanadia catalysts [19]. Thus, it is conceivable that the desorption of target product of C_3H_6 would be facile over the V-SBA catalyst without surface medium acid sites.

Isolated tetrahedral V^{5+} species appear to be the selective sites in the oxidative dehydrogenation of propane, as previously proposed in V-MCM-41 systems, V-containing microporous materials, or supported vanadia catalysts [5,12, 17,32]. The polymerization degree of the surface vanadia species and the appearance of V_2O_5 crystallites have a significant effect on the selectivity to propylene. As has been suggested, the surface propyl species or adsorbed propylene may react over two V atoms of V–O–V species favoring the consecutive reactions and decreasing the selectivity to propylene from propane [6,62]. Thus, the present superior performance of the V-SBA catalysts in the oxidative dehydrogenation of propane is a consequence of the greater density of active species with a lower surface acidity achieved on the surface of the SBA-15 support as suggested from the detailed characterization results presented above.

5. Conclusions

This work presents a detailed study of the effect of V content on the nature of the VO_x species anchored on the surface of the SBA-15-supported vanadia catalysts. The results show that the V-containing SBA-15 catalysts possess a unique textural feature of high surface area as well as the well-organized mesoporous structures with large pore diameters. The comparative study of the V-SBA and V-MCM-41 and the conventional V–SiO_2 catalysts has shown that a higher concentration of isolated V species is readily achievable on the surface of the SBA-15 support. Moreover, a much weaker and lower acidity of the surface acid sites is observed for the vanadium-incorporated SBA-15 catalysts. The high dispersion of vanadium species achievable on the SBA-15 support with large pore diameters as well as the relatively low surface acidity of the catalyst is considered to be responsible for the superior catalytic behavior of the V-SBA catalyst in the oxidative dehydrogenation of propane.

Acknowledgments

This work was supported by the National Major Basic Research Program of China (Grant 2003CB615807), the National Science Foundation of China (Grant 20203003), and the Committee of Shanghai Science and Technology (Grant 02QA14006).

References

[1] H.H. Kung, Adv. Catal. 1 (1994) 40.
[2] T. Blasco, J.M.L. Nieto, Appl. Catal. A 157 (1997) 117.
[3] S. Sugiyama, Y. Iozuka, E. Nitta, H. Hayashi, J.B. Moffat, J. Catal. 189 (2000) 233.
[4] M.M. Bettahar, G. Costentin, L. Savary, J.C. Lavalley, Appl. Catal. A 145 (1996) 1.
[5] J. Santamaría-González, J. Luque-Zambrana, J. Mérida-Robles, P. Maireles-Torres, E. Rodríguez-Casllón, A. Jiménez-López, Catal. Lett. 68 (2000) 67.
[6] M. Chaar, D. Patel, M. Kung, H.H. Kung, J. Catal. 109 (1988) 463.

[7] F. Arena, F. Frusteri, A. Parmaliana, G. Martra, S. Coluccia, Stud. Surf. Sci. Catal. 119 (1998) 665.
[8] A. Khodakov, J. Yang, S. Su, E. Iglesia, A.T. Bell, J. Catal. 177 (1998) 343.
[9] A. Khodakov, B. Olthof, A.T. Bell, E. Iglesia, J. Catal. 181 (1999) 205.
[10] M. Puglisi, F. Arena, F. Frusteri, V. Sokolovskii, A. Parmaliana, Catal. Lett. 41 (1996) 41.
[11] C. Pak, A.T. Bell, T.D. Tilley, J. Catal. 206 (2002) 49.
[12] R. Zhou, Y. Cao, S.R. Yan, J.F. Deng, Y.Y. Liao, B.F. Hong, Catal. Lett. 75 (2001) 107.
[13] J.S. Beck, J.C. Vartuli, W.J. Roth, M.E. Leonowicz, C.T. Kresge, K.D. Schmitt, C.T.W. Chu, D.H. Olsen, E.W. Sheppard, S.B. McCullen, J.B. Higgins, J.L. Schlenker, J. Am. Chem. Soc. 114 (1992) 10834.
[14] A. Corma, Chem. Rev. 97 (1997) 2373.
[15] O.V. Buyevskaya, A. Bruckner, E.V. Kondratenko, D. Wolf, M. Baerns, Catal. Today 67 (2001) 369.
[16] J. Santamaria-Gonzalez, J. Luque-Zambrana, J. Merida-Robles, P. Maireles-Torres, E. Rodriguez-Castellon, A. Jimenez-Lopez, Catal. Lett. 68 (2000) 67.
[17] M.L. Peña, A. Dejoz, V. Fornés, E. Rey, M.I. Vázquez, J.M. López Nieto, Appl. Catal. A 209 (2001) 155.
[18] Y. Wang, Q.H. Zhang, Y. Ohishi, T. Shishido, K. Takehira, Catal. Lett. 72 (2001) 215.
[19] Q. Zhang, Y. Wang, Y. Ohishi, T. Shihido, K. Takehira, J. Catal. 202 (2001) 308.
[20] B. Solsona, T. Blasco, J.M.L. Nieto, M.L. Peña, F. Rey, A. Vidal-Moya, J. Catal. 203 (2001) 443.
[21] D.Y. Zhao, J.L. Feng, Q.S. Huo, N. Melosh, G.H. Fredrickson, B.F. Chmelka, G.D. Stucky, Science 279 (1998) 548.
[22] V. Dufaud, M.E. Davis, J. Am. Chem. Soc. 125 (2003) 9403.
[23] B.M. Lin, X.X. Wang, Q. Guo, W. Yang, Q.H. Zhang, Y. Wang, Chem. Lett. 32 (2003) 860.
[24] Y. Cao, J.C. Hu, P. Yang, W.L. Dai, K.N. Fan, Chem. Commun. (2003) 908.
[25] V. Fornés, C. López, H.H. López, A. Martinez, Appl. Catal. A 249 (2003) 345.
[26] L. Vradman, M.V. Landau, M. Herskowitz, V. Ezersky, M. Talianker, S. Nikitenko, Y. Koltypin, A. Gedanken, J. Catal. 213 (2003) 163.
[27] J. Jarupatrakorn, T.D. Tilley, J. Am. Chem. Soc. 124 (2002) 8380.
[28] Y.M. Liu, Y. Cao, K.K. Zhu, S.R. Yan, W.L. Dai, H.Y. He, K.N. Fan, Chem. Commun. (2002) 2832.
[29] Y.M. Liu, Y. Cao, S.R. Yan, W.L. Dai, K.N. Fan, Catal. Lett. 88 (2003) 61.
[30] A. Davydov, in: N.T. Sheppard (Ed.), Molecular Spectroscopy of Oxide Catalyst Surfaces, Wiley, Chichester, 2003, p. 5.
[31] R. Zhou, Y. Cao, S.R. Yan, K.N. Fan, Appl. Catal. A 236 (2002) 103.
[32] W.Z. Weng, M.S. Chen, Q.G. Yan, T.H. Wu, Z.S. Chao, Y.Y. Liao, H.L. Wan, Catal. Today 63 (2000) 317.
[33] H. Berndt, A. Martin, A. Brückner, E. Schreier, D. Müller, H. Kosslick, G.-U. Wolf, B. Lücke, J. Catal. 191 (2000) 384.
[34] C.B. Wang, G. Deo, I.E. Wachs, J. Catal. 178 (1998) 640.
[35] D. Wei, H. Wang, X. Feng, W.T. Chueh, P. Ravikovitch, M. Lyubovsky, C. Li, T. Takeguchi, G.L. Haller, J. Phys. Chem. B 103 (1999) 2113.
[36] M. Baltes, K. Cassiers, P. Van der Voort, B.M. Weckhuysen, R.A. Schoonheydt, E.F. Vansant, J. Catal. 197 (2001) 160.
[37] K. Chen, E. Iglesia, A.T. Bell, J. Catal. 192 (2000) 197.
[38] J.L. Male, H.G. Niessen, A.T. Bell, T.D. Tilley, J. Catal. 194 (2000) 431.
[39] H. Eckert, I.E. Wachs, J. Phys. Chem. 93 (1989) 6796.
[40] O.B. Lapina, V.M. Mastikhin, A.A. Shubin, V.N. Krasilnikov, K.I. Zamarev, Prog. Nucl. Magn. Reson. Spectrosc. 24 (1992) 457.
[41] N. Das, H. Eckert, H. Hu, I.E. Wachs, J.F. Walzer, F.J. Feher, J. Phys. Chem. 97 (1993) 8240.
[42] T. Blasco, A. Dejoz, J.M. López Nieto, M.I. Vázquez, J. Catal. 157 (1995) 271.
[43] O.B. Lapina, V.M. Mastikhin, L.G. Simonova, Yu.O. Bulgakova, J. Mol. Catal. 69 (1991) 61.
[44] T. Blasco, A. Galli, J.M. López Nieto, F. Trifiró, J. Catal. 169 (1997) 203.
[45] P.C. Stair, C. Li, J. Vac. Sci. Technol. A 15 (1997) 1679.
[46] C. Li, G. Xiong, Q. Xin, J. Liu, P. Ying, Z. Feng, J. Li, W. Yang, Y. Wang, G. Wang, X. Liu, M. Lin, X. Wang, E. Min, Angew. Chem., Int. Ed. Engl. 38 (1999) 2220.
[47] Y.T. Chua, P.C. Stair, I.E. Wachs, J. Phys. Chem. B 105 (2001) 8600.
[48] G. Xiong, C. Li, Z. Feng, P. Ying, Q. Xin, J. Liu, J. Catal. 186 (1999) 234.
[49] G. Xiong, C. Li, H. Li, Q. Xin, Z. Feng, Chem. Commun. (2000) 677.
[50] G.T. Went, S.T. Oyama, A.T. Bell, J. Phys. Chem. 94 (1990) 4240.
[51] H. Kosslick, G. Lischke, G. Walther, W. Storek, A. Martin, R. Fricke, Micropor. Mater. 9 (1997) 13.
[52] E.P. Parry, J. Catal. 2 (1963) 371.
[53] G. Grubert, J. Rathouský, G. Schulz-Ekloff, M. Wark, A. Zukal, Micropor. Mesopor. Mater. 22 (1998) 225.
[54] C.A. Grande, A.E. Rodrigues, Ind. Eng. Chem. Res. 40 (2001) 1686.
[55] G. Centi, F. Fazzani, L. Canesson, A. Tuel, Stud. Surf. Sci. Catal. 110 (1997) 893.
[56] S. Lim, G.L. Haller, Appl. Catal. A 188 (1999) 277.
[57] L. Owens, H.H. Kung, J. Catal. 144 (1993) 202.
[58] M. Bañares, X. Cao, J.L.G. Fierro, I.E. Wachs, Stud. Surf. Sci. Catal. 110 (1997) 295.
[59] G. Centi, S. Perhatoner, F. Trifiró, A. Aboukais, C.F. Aissi, M. Guelton, J. Phys. Chem. 96 (1992) 2617.
[60] G. Centi, F. Trifiró, Appl. Catal. A 143 (1996) 3.
[61] S. Dzwigaj, M. Matsuoka, M. Anpo, M. Che, J. Phys. Chem. B 104 (2000) 6012.
[62] A. Corma, J.M. López Nieto, N. Paredes, M. Perez, Y. Shen, H. Cao, S.L. Suib, Stud. Surf. Sci. Catal. 72 (1992) 213.